

Low Dimensional and Frustrated Antiferromagnetic Interactions in Transition Metal Chloride Complexes with Simple Amine Ligands

James E. Chalmers,^a Anant Kumar Srivastava,^a
Richard J. C. Dixey,^a Krrishna Sivakumaran^a and
Paul J. Saines^{*a}

^aSchool of Physical Sciences, Ingram Building
University of Kent
Canterbury CT2 7NH

Electronic Supplementary Information

Hydrogen Bonding Networks in the Discrete Hydrazinium Complexes

The shortest hydrogen bond contacts between layers in $\text{Hyd}_2\text{CoCl}_4$ involve the hydrogen atoms bonded to the N2 atom, with three N2...Cl contacts at distances between 3.163(8) and 3.253(4) Å, while one of the hydrogen atoms bonded to the N1 atom, which is coordinated to Co, has a hydrogen bond with a N1...Cl contact at 3.261(3) Å. A hydrogen atom bonded to each of the N1 and N2 atoms have one additional hydrogen bond with a Cl⁻ anion from a different complex in the same layer with N1...Cl and N2...Cl distances of 3.404(10) and 3.164(4) Å; the later appears to be bifurcated hydrogen bond with the water molecule on the same complex with a N2...O contact of 3.275(5) Å. The two hydrogen atoms from the oxygen atom of the water molecule form hydrogen bonds to the Cl between layers with an O...Cl contact of 3.184(4) Å and to the octahedra on the opposite side of a rhombohedra in the same layer with an O...Cl contact of 3.245(10) Å.

The high Cl and NH_3NH_2^+ content of $\text{Hyd}_3\text{MnCl}_5$ leads to a highly complex hydrogen bond network, the majority of which involve the Cl ligands. The NH_3NH_2 ligand coordinated to the Mn atom has single hydrogen bonds between the hydrogen atoms bonded to N1, the atom to which the Mn is coordinated, and Cl atoms with N1...Cl contacts at 3.3043(19) and 3.444(2) Å while the hydrogen atoms bonded to N2 form hydrogen bond with the two uncoordinated NH_3NH_2^+ cations at 2.904(3) and 2.945(4) Å and one Cl atom at 3.340(4) Å. In contrast the hydrogen bonds from the uncoordinated NH_3NH_2^+ cations appear to only be with the Cl atoms with most hydrogen atoms involved in bifurcated bonds, with two centred hydrogen bonds having N...Cl distances of less than 3.3 Å.

There is an intricate hydrogen-bonding network between complexes in HydMnCl_3 . The hydrogen atoms from the N2 atom of the NH_3NH_2 ligand, have three hydrogen bonds with Cl ligands with N...Cl distances between 3.189(2) and 3.255(3) Å, one of which is bifurcated with a contact with the H_2O molecule with an N...O distance of 3.014(3) Å. One of the hydrogen atoms bonded to N1, which is coordinated to the Mn cation, appears to have a bifurcated hydrogen bond with a Cl ligand from another complex, with N...Cl distances of 3.288(2) and 3.412(3) Å. Both of the distinct water molecules have two hydrogen bonds with neighbouring Cl atoms with distances of 3.199(2) and 3.212(2) Å for O1...Cl and 3.179(2) and 3.256(2) Å for O2...Cl, respectively.

$\text{Hyd}_{10}\text{Mn}_3\text{Cl}_{16}$ has the most complex hydrogen bond network of these four compounds as might be expected giving is low symmetry. Cl atoms primarily act as acceptors with every Cl atom in the structure involved in at least three hydrogen bonds with a maximum of seven for the one distinct free Cl⁻ anion. The number of hydrogen bonds that do not involve Cl atoms are much more restricted with less than 10 % of the hydrogen bonds involving free NH_3NH_2^+ cations not involving Cl ligands, being to free NH_3NH_2^+ cations (in two cases) and the bound H_2O water molecules (in one case). Unlike the free NH_3NH_2^+ , where about two-thirds of the hydrogen atoms appear to be involved in bifurcated bonds, all of the hydrogen atom from ligands are involved in only one hydrogen bond. For the H_2O molecule one hydrogen atom is involved in a hydrogen bond to the free Cl anion (O...Cl distance of 3.129(8) Å) and one coordinated Cl atom (3.196(5) Å) that is coordinated to a Mn atom in an adjacent layer. Similarly the two hydrogen atoms bonded to the N through which the bound NH_3NH_2 ligands coordinate to the Mn atoms, are involved in a hydrogen bond to the free Cl⁻ anion (N...Cl distance of 3.340(7) Å) and a bound chloride (3.340(7) Å), in this case that is coordinated to an Mn1 octahedra in an adjacent layer. The three hydrogen atoms bonded to the other N atom in the bound NH_3NH_2 ligands are involved in hydrogen bonds to two distinct free NH_3NH_2^+ cations (N...N distances of 2.900(6) Å and 2.958(4) Å).

Å) and one Cl ligand (N...Cl distance of 3.181(9) Å) that is coordinated to a different Mn1Cl₆ octahedra from an adjacent layer than the other end of the NH₃NH₂ molecule is hydrogen bonded to.

Powder X-ray Diffraction

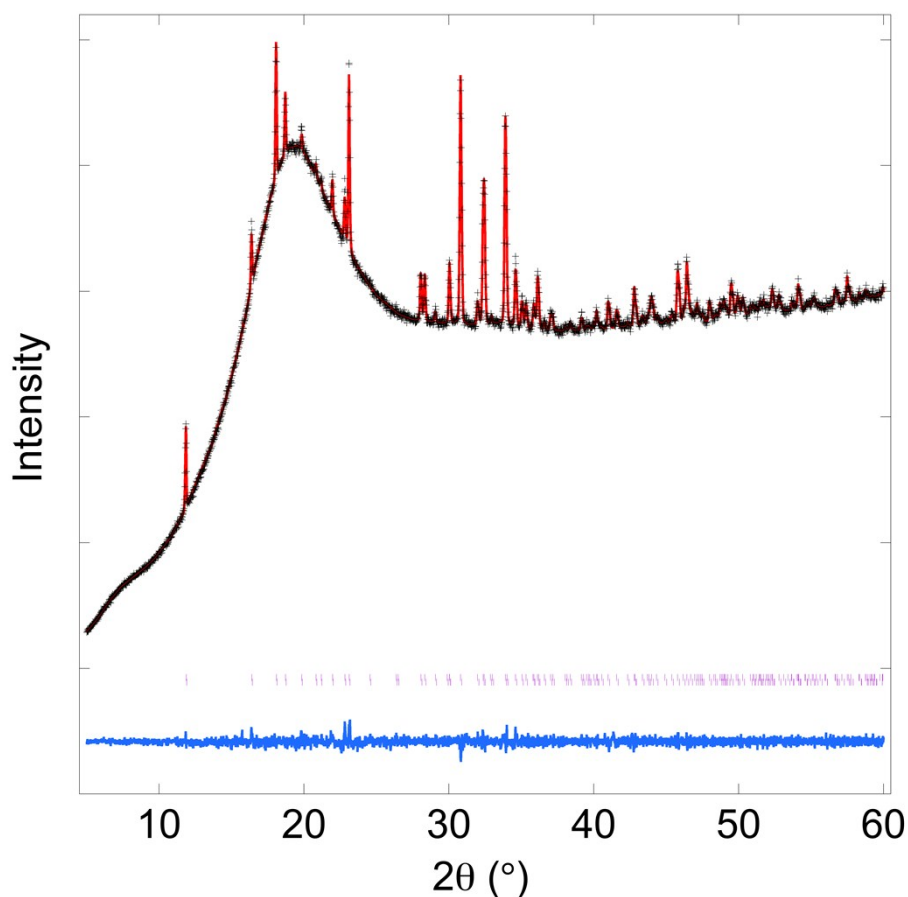


Fig. S1: Le Bail fit to a powder X-ray diffraction pattern of Hyd₂CoCl₄. The experimental data are shown as black crosses, the calculated fit as a red line, the difference plot as a blue line and the expected position of Bragg reflections as purple vertical lines. The broad peak centred at about 20° is caused by the plastic sample holder. The R_p , R_{wp} and χ^2 are 0.62 %, 0.81 % and 0.99 and unit cell parameters of $a = 8.0066(3)$ Å, $b = 5.7193(2)$ Å, $c = 11.4084(4)$ Å, $\beta = 97.6773(18)^\circ$ and volume = 517.74(3) Å³.

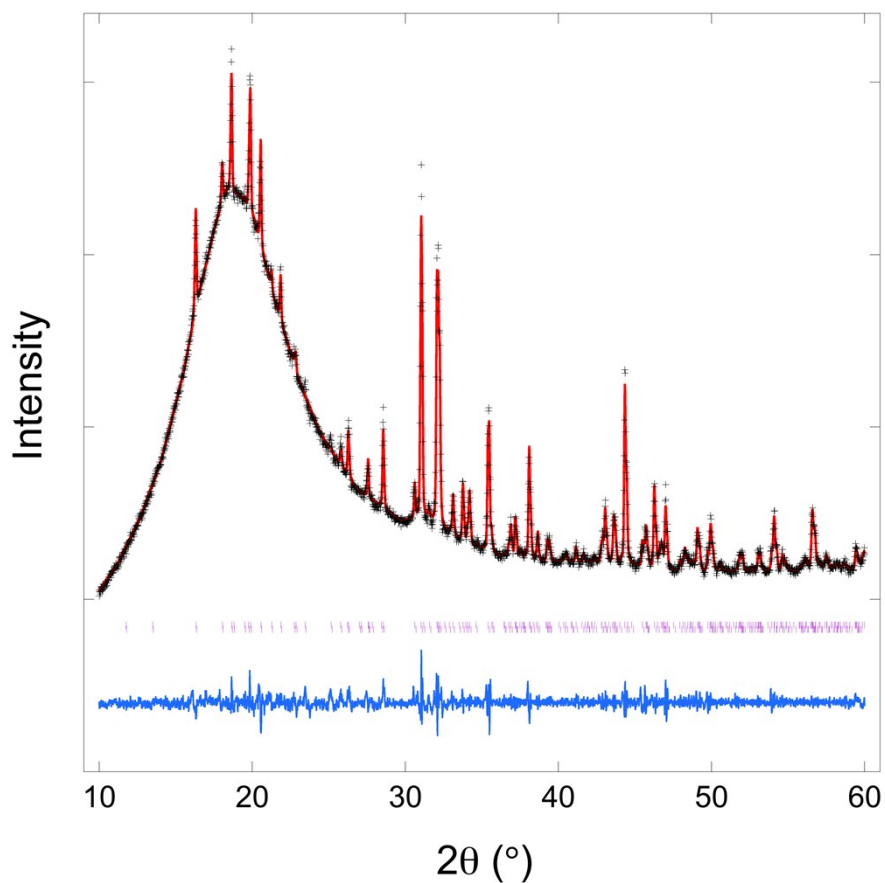


Fig. S2: Le Bail fit to a powder X-ray diffraction pattern of HydMnCl_3 . The format is the same as in Fig. S1 and the broad peak centred at about 20° is caused by the plastic sample holder. The R_p , R_{wp} and χ^2 are 1.20 %, 1.69 % and 2.37 and unit cell parameters of $a = 5.5529(3) \text{ \AA}$, $b = 14.0057(7) \text{ \AA}$, $c = 9.9747(5) \text{ \AA}$, $\beta = 92.613(2)^\circ$ and volume = $774.96(7) \text{ \AA}^3$.

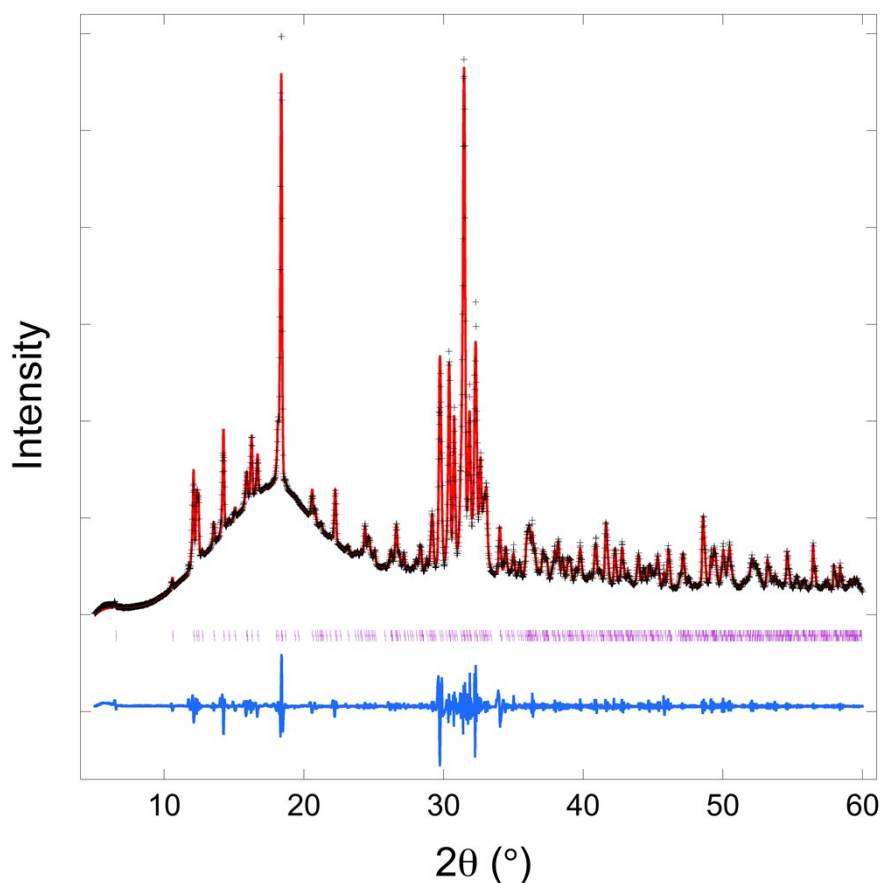


Fig. S3: Le Bail fit to a powder X-ray diffraction pattern of $\text{Hyd}_{10}\text{Mn}_3\text{Cl}_{16}$. The format is the same as in Fig. S1 and the broad peak centred at about 20° is caused by the plastic sample holder. The R_p , R_{wp} and χ^2 are 1.20 %, 2.18 % and 87.51 and unit cell parameters of $a = 7.6038(3) \text{ \AA}$, $b = 9.1915(3) \text{ \AA}$, $c = 15.0771(7) \text{ \AA}$, $\alpha = 89.786(3)^\circ$, $\beta = 84.355(3)^\circ$, $\gamma = 75.580(2)^\circ$ and volume = $1015.4(7) \text{ \AA}^3$.

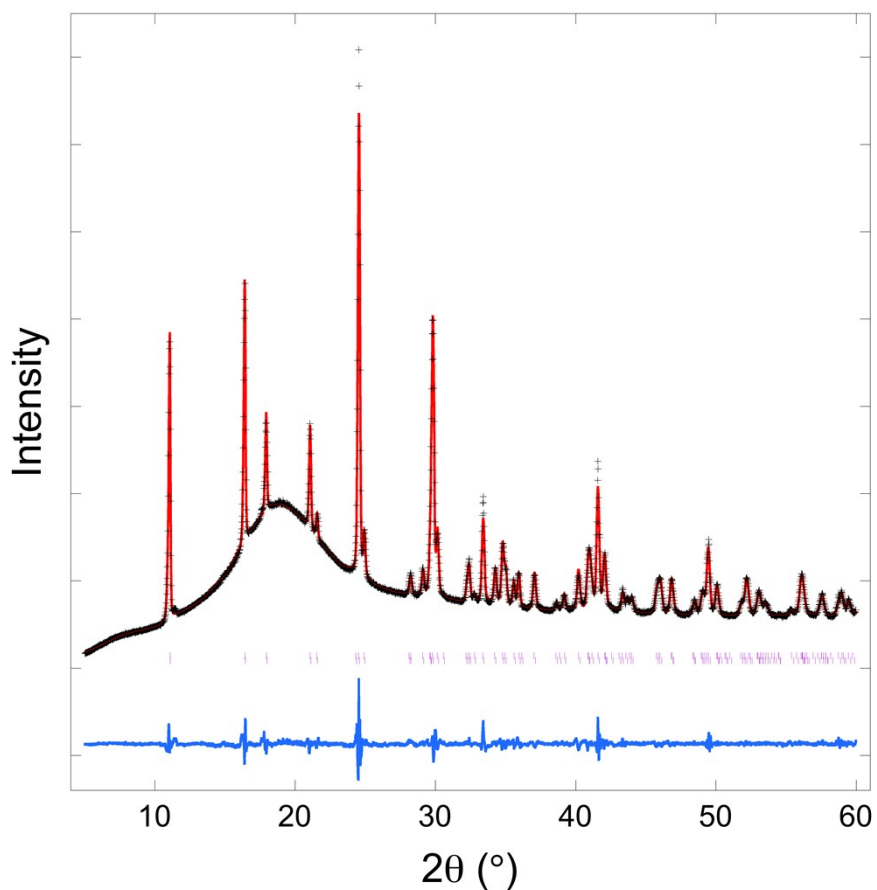


Fig. S4: Le Bail fit to a powder X-ray diffraction pattern of $\text{MHA}_2\text{CuCl}_2$. The format is the same as in Fig. S1 and the broad peak centred at about 20° is caused by the plastic sample holder. The R_p , R_{wp} and χ^2 are 1.94 %, 2.81 % and 7.92 and unit cell parameters of $a = 3.81978(14) \text{ \AA}$, $b = 5.7298(2) \text{ \AA}$, $c = 8.7638(3) \text{ \AA}$, $\alpha = 99.699(2)^\circ$, $\beta = 98.879(3)^\circ$, $\gamma = 92.481(3)^\circ$ and volume = $186.33(13) \text{ \AA}^3$.

Infra-red Spectra

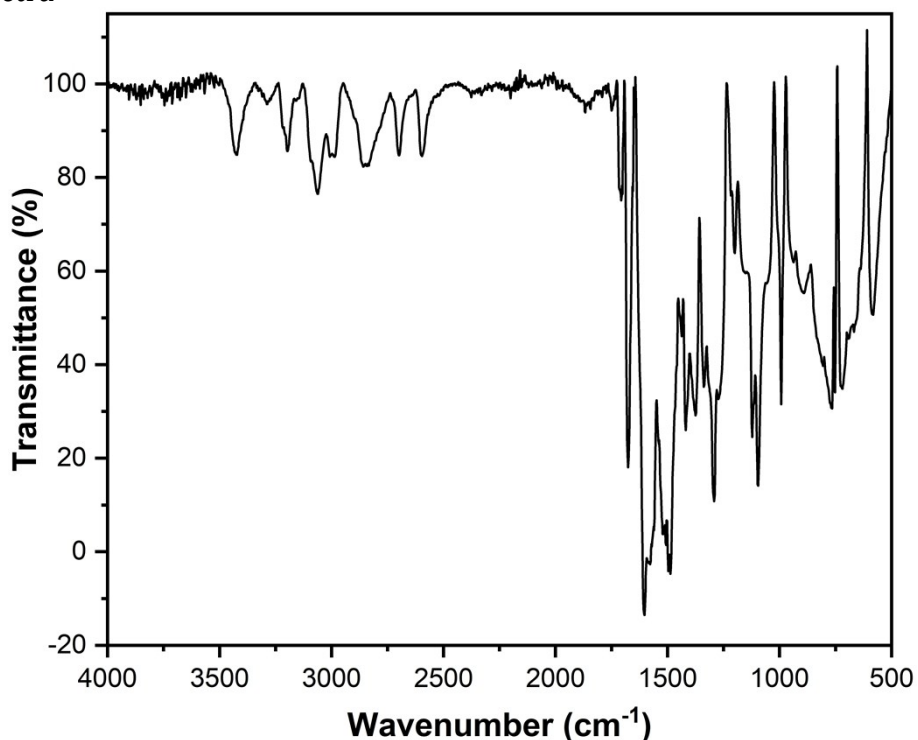


Fig. S5: Solid-state FT-IR spectra of Hyd₂CoCl₄. Infra-red features are observed at (in cm⁻¹) 3423 (O-H stretch), 3286, 3196, 3145, 3092, 3062, 3007, 2986 (N-H stretch), 2858, 2841, 2698, 2600, 1676, 1602, 1578 (N-H bend), 1506, 1496, 1487, 1437, 1419, 1375, 1338 (O-H bend), 1292, 1271, 1217, 1199, 1122, 1095, 993, 943, 910, 806, 775, 754, 715, 654, 636, 582 (metal-ligand interactions).

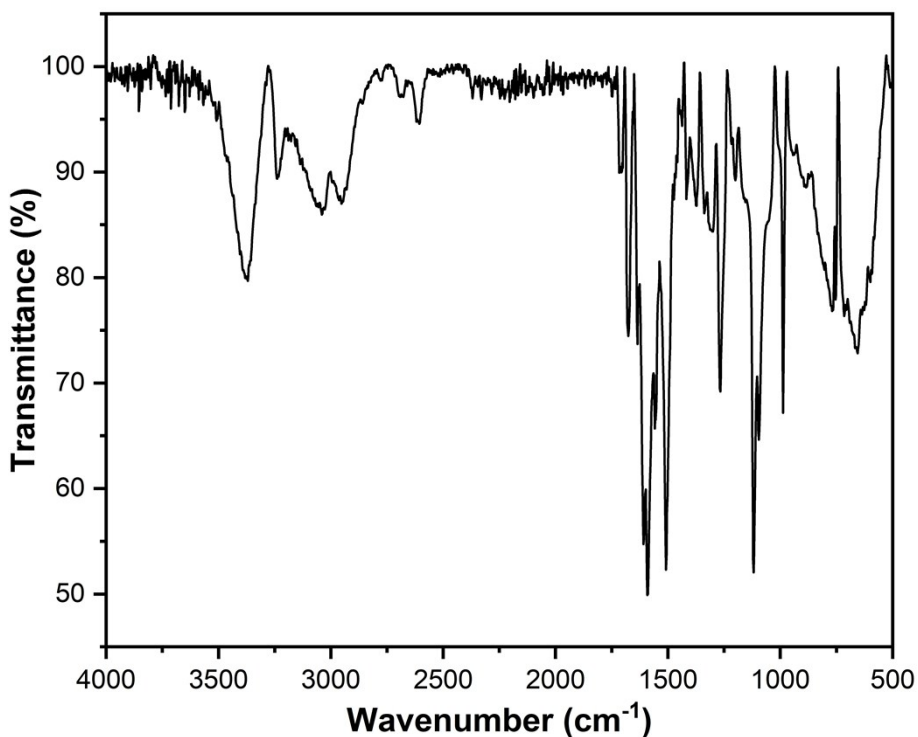


Fig. S6: Solid-state FT-IR spectra of HydMnCl₃. Infra-red features are observed at (in cm⁻¹) 3375 (O-H stretch), 3238, 3040, 2953 (N-H stretch), 2777, 2690, 2605, 1716, 1676, 1635, 1608, 1591 (N-H bend), 1558, 1508, 1437, 1417, 1373, 1338 (O-H bend), 1302, 1267, 1217, 1199, 1118, 1095, 987, 950, 908, 894, 769, 754, 729, 652, 617, 592, 547 (metal-ligand interactions).

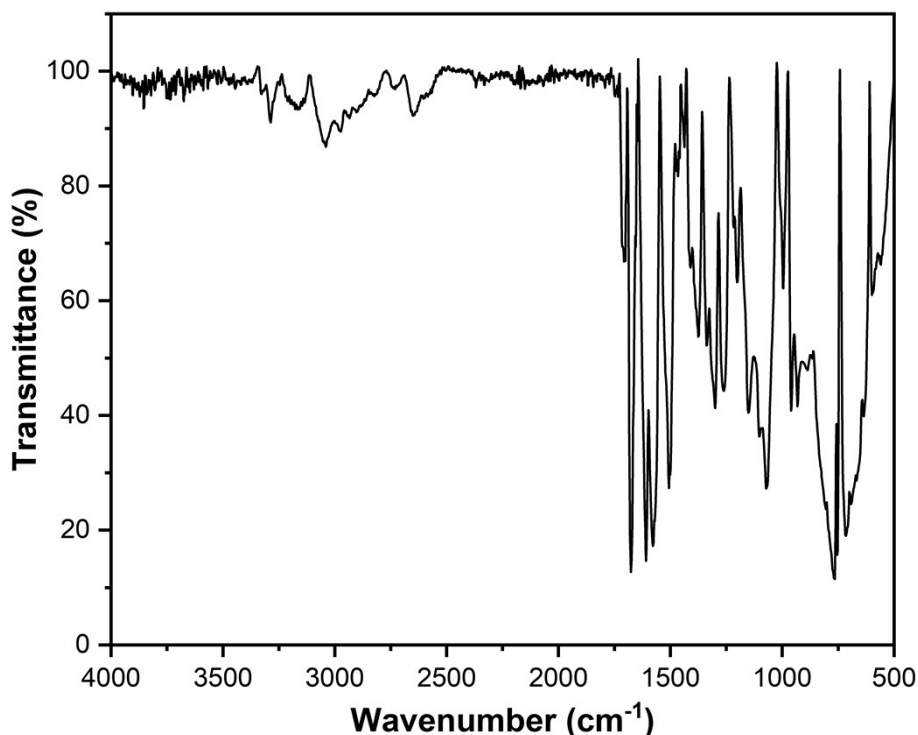


Fig. S7: Solid-state FT-IR spectra of $\text{Hyd}_{10}\text{Mn}_3\text{Cl}_{16}$. Infra-red features are observed at (in cm^{-1}) 3327 (O-H stretch), 3286, 3157, 3040, 2972 (N-H stretch), 2933, 2902, 2746, 2644, 1676, 1606, 1568 (N-H bend), 1506, 1466, 1437, 1410, 1375, 1338 (O-H bend), 1300, 1261, 1217, 1199, 1147, 1101, 1066, 995, 960, 932, 814, 775, 754, 706, 654, 634, 542 (metal-ligand interactions).

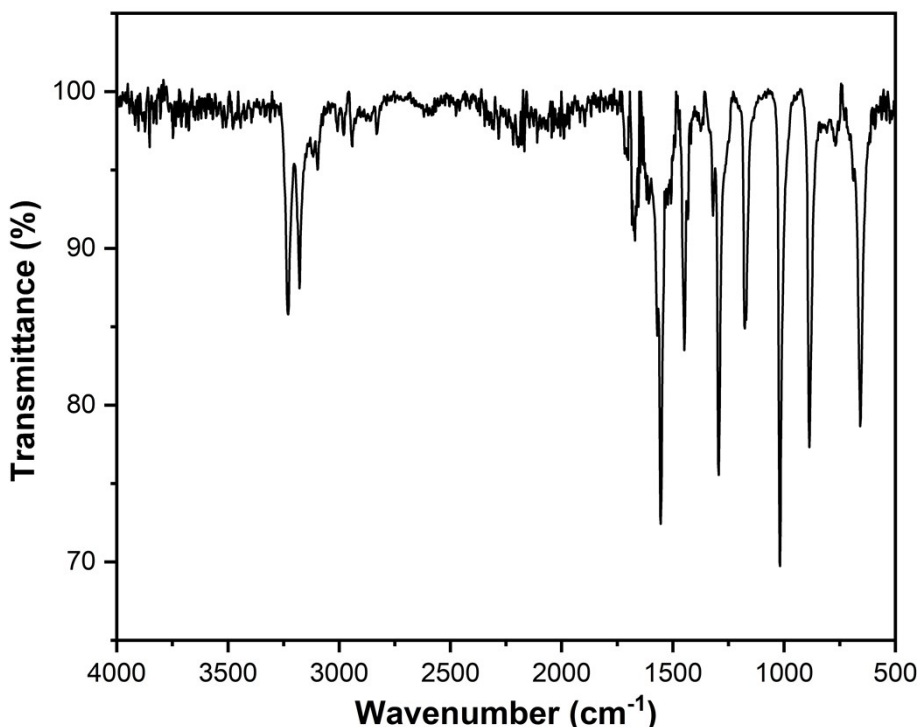


Fig. S8: Solid-state FT-IR spectra of $\text{MHA}_2\text{CuCl}_2$. Infra-red features are observed at (in cm^{-1}) 3228, 3178, 3116, 3097, 3007, 2980 (N-H stretch), 2941, 2831 (C-H stretch), 1716, 1701, 1670, 1608, 1570 (N-H bend), 1544, 1508, 1448, 1433, 1375, 1319, 1294, 1178 (C-O stretch), 1018, 887, 769, 729, 705, 688, 657, 592, 561, 511 (C-H bend and metal-ligand interactions).

Crystallographic Depictions

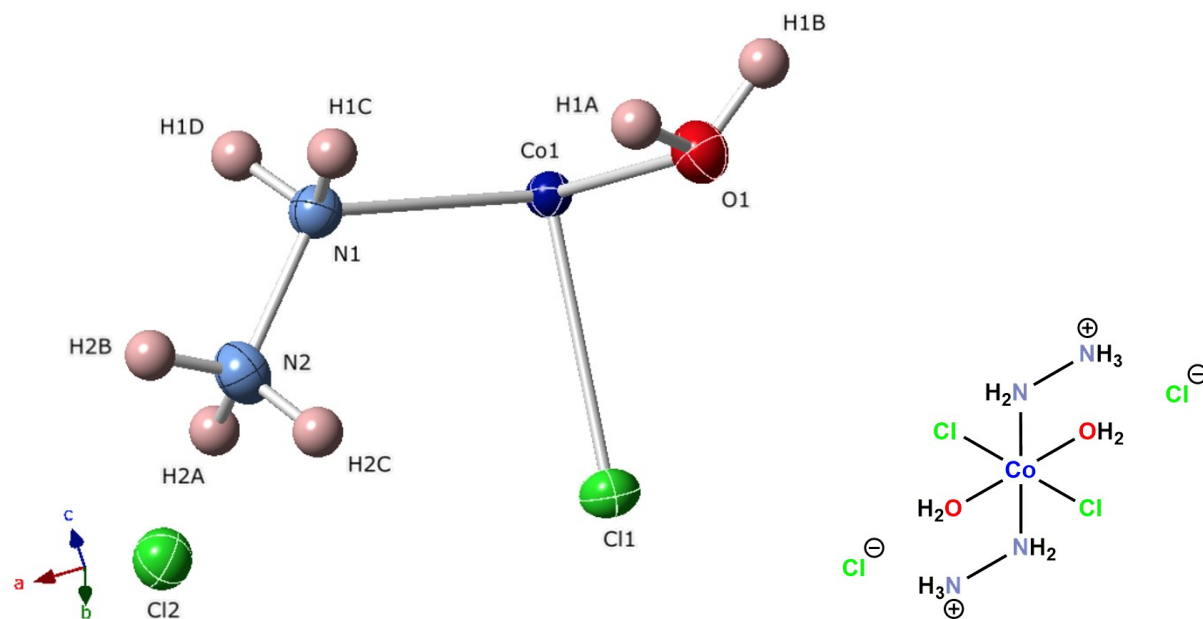


Fig. S9: Asymmetric unit of $\text{Hyd}_2\text{CoCl}_4$ with displacement ellipsoids shown at the 50 % probability level. The Co, N, O, Cl and H atoms are shown as dark blue, light blue, red, green and light pink spheres, respectively. For clarity a schematic drawing of the complex is shown on the right-hand side of the figure.

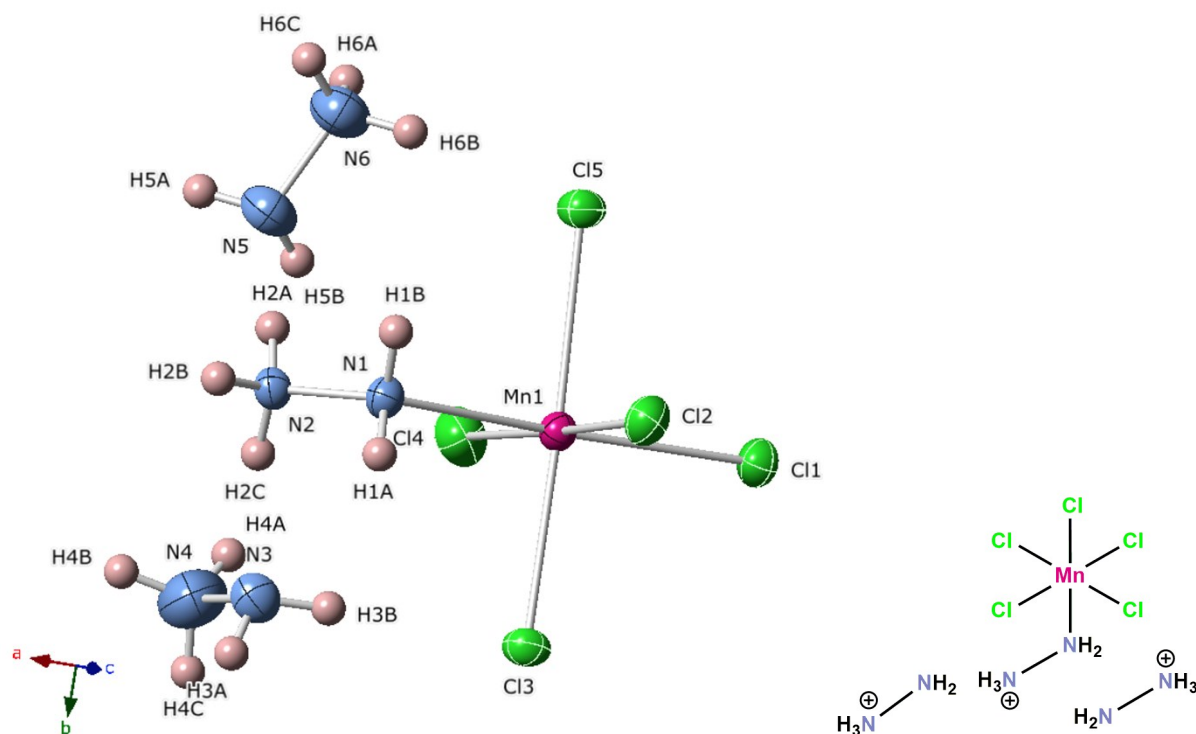


Fig. S10: Asymmetric unit of $\text{Hyd}_3\text{MnCl}_5$ with displacement ellipsoids shown at the 50 % probability level. The Mn are shown as dark pink spheres and all other colours are as in Fig. S9. For clarity a schematic drawing of the complex is shown on the right-hand side of the figure.

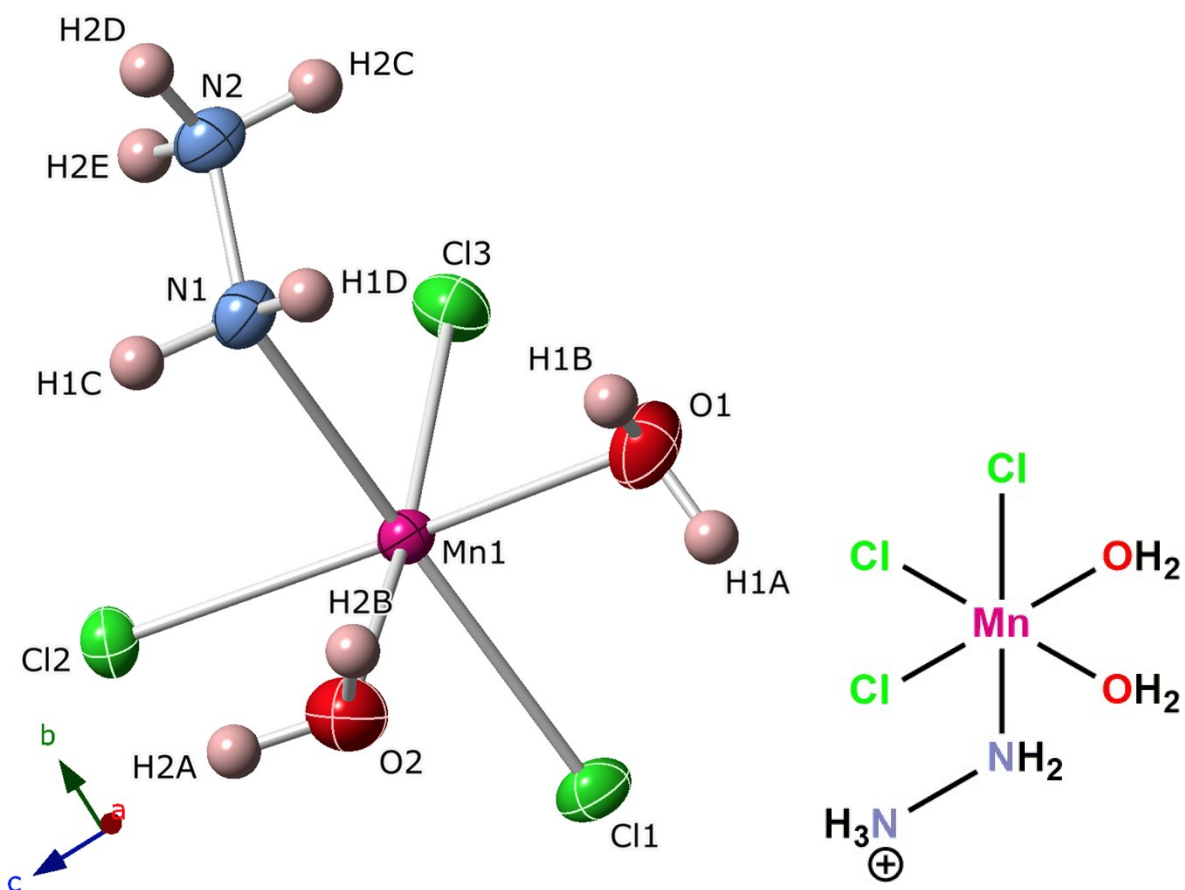


Fig. S11: Asymmetric unit of HydMnCl₃ with displacement ellipsoids shown at the 50 % probability level. The colours are as in Fig. S10. For clarity a schematic drawing of the complex is shown on the right-hand side of the figure.

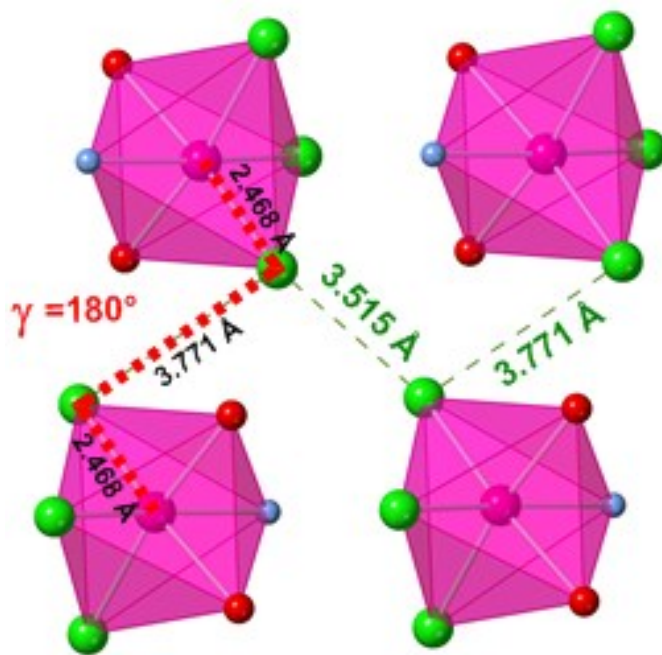


Fig. S12: Section of the crystal structure of HydMnCl₃ showing the Cl...Cl contacts within the zig-zag chain with the shortest magnetic coupling pathways. All Mn-Cl...Cl-Mn torsion angles in this chain are 180° so only one is shown for clarity.

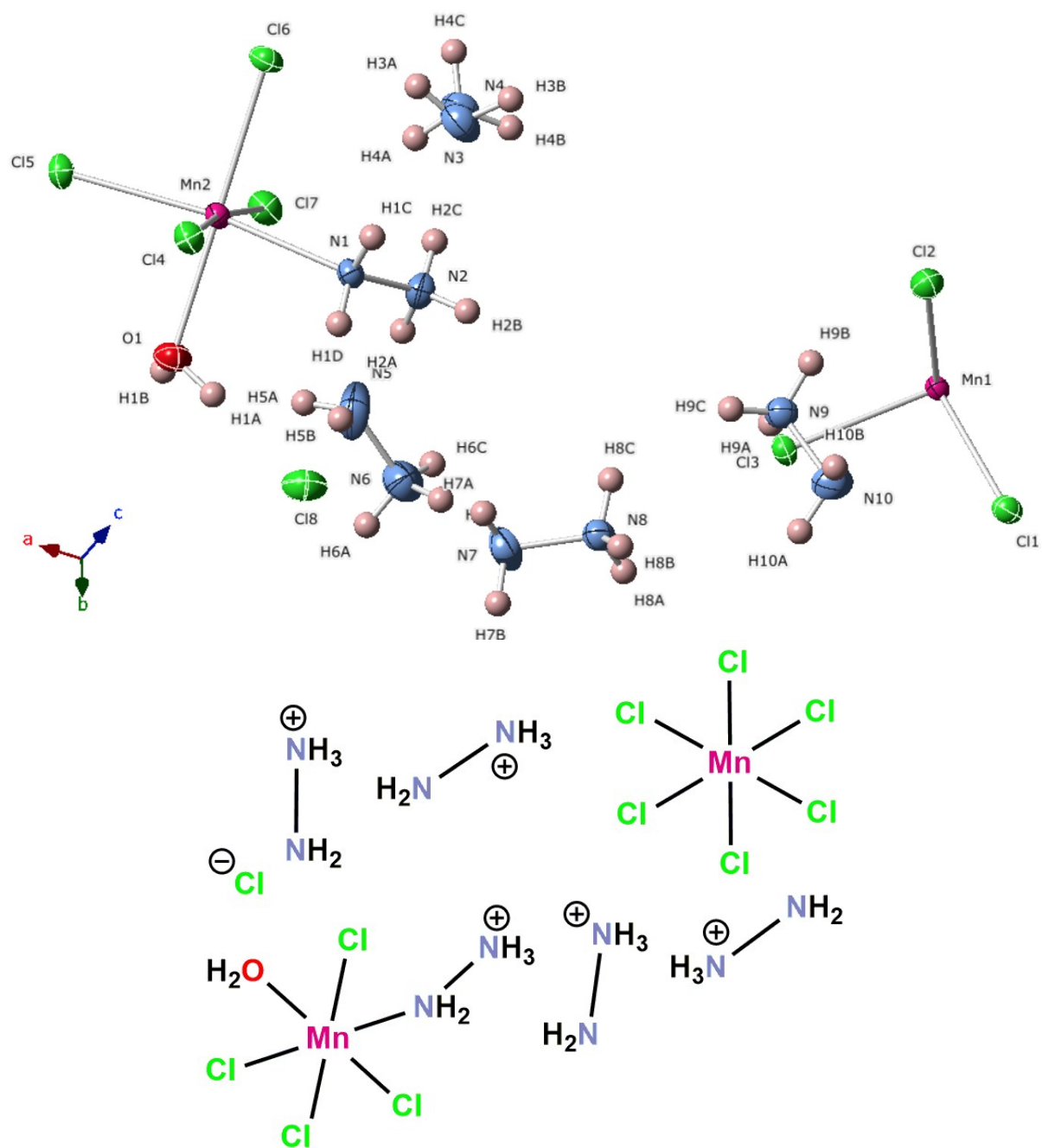


Fig. S13: Asymmetric unit of $\text{Hyd}_{10}\text{Mn}_3\text{Cl}_{16}$ with displacement ellipsoids shown at the 50 % probability level. The colours are as in Fig. S10. For clarity a schematic drawing of the complex is shown at the bottom of the figure.

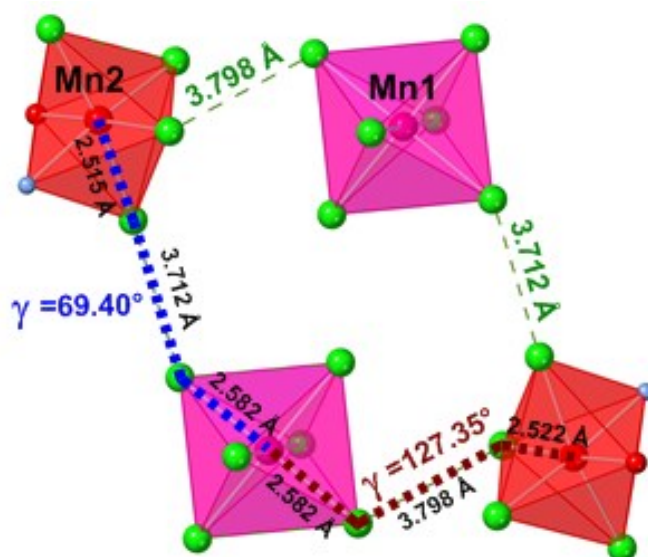


Fig. S14: Section of the crystal structure of $\text{Hyd}_{10}\text{Mn}_3\text{Cl}_{16}$ showing the Cl...Cl contacts within the rhombohedra and the corresponding Mn-Cl...Cl-Mn torsion distances.

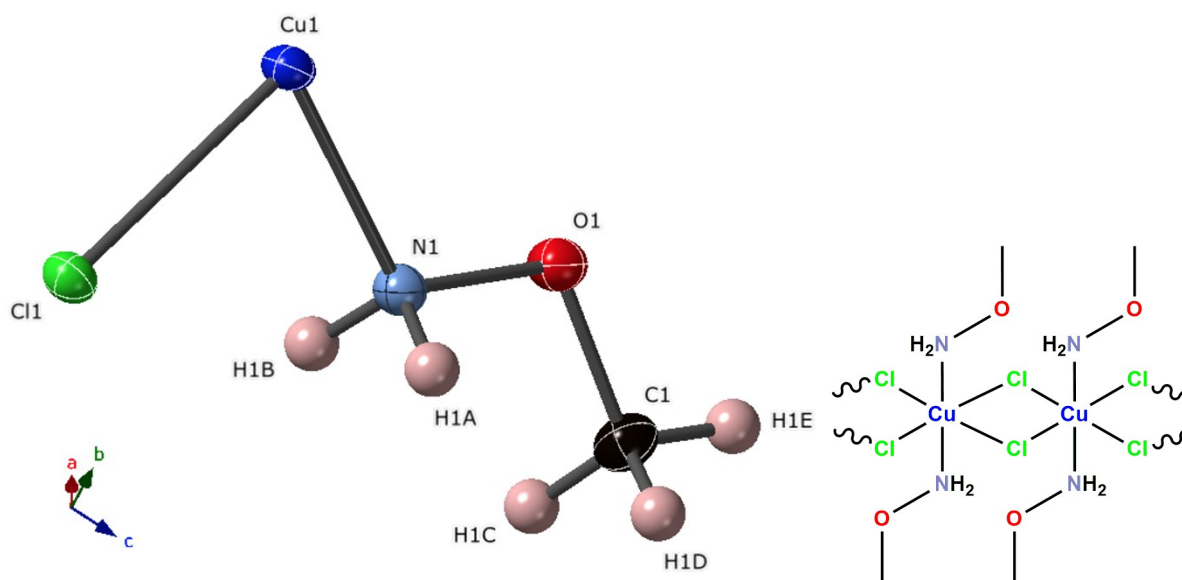


Fig. S15: Asymmetric unit of $\text{MHA}_2\text{CuCl}_2$ with displacement ellipsoids shown at the 50% probability level. The Cu cations are shown in dark blue and all other colours are as in Fig. S9. For clarity a schematic drawing of the compound is shown on the right-hand side of the figure.

Thermal Analysis

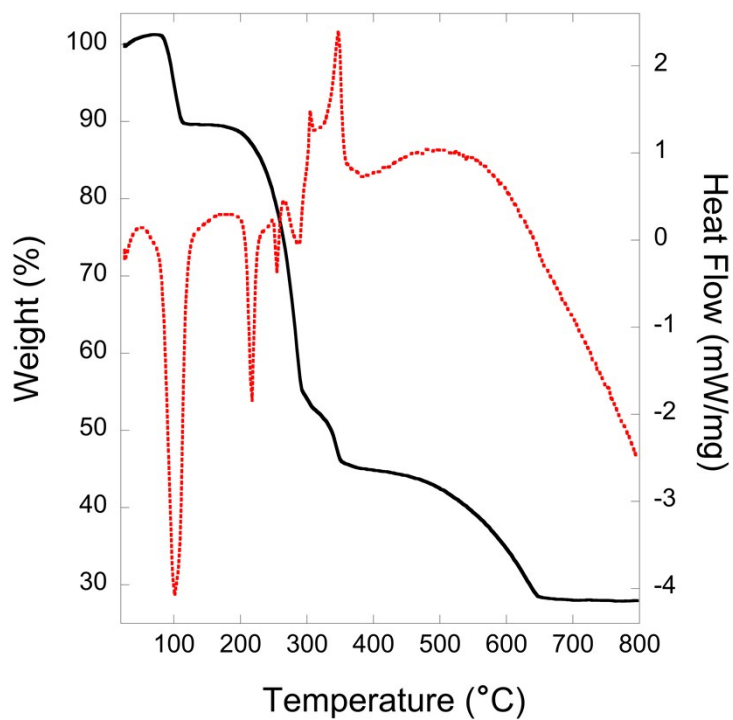


Fig. S16: Thermogravimetric (continuous black line) and differential thermal (dotted red line) analysis obtained from $\text{Hyd}_2\text{CoCl}_4$ in air.

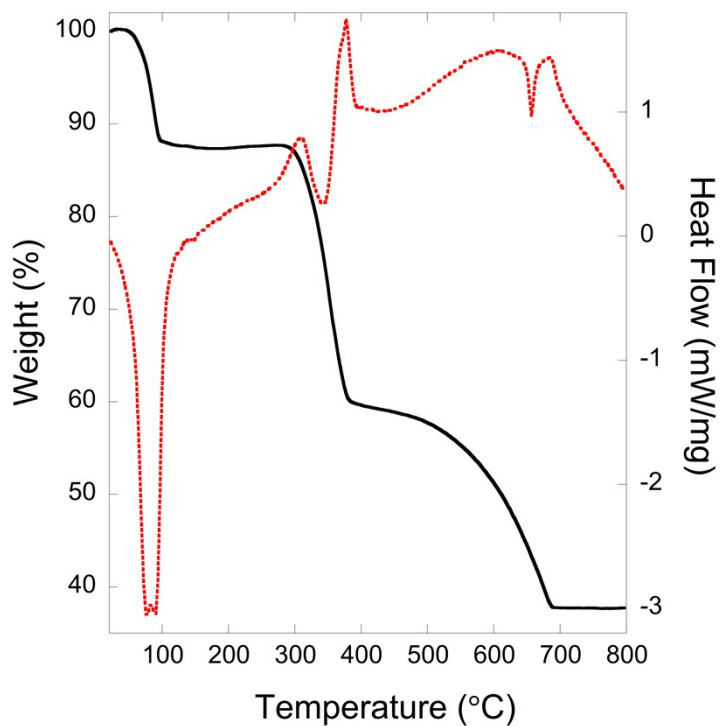


Fig. S17: Thermogravimetric (continuous black line) and differential thermal (dotted red line) analysis obtained from HydMnCl_3 in air.

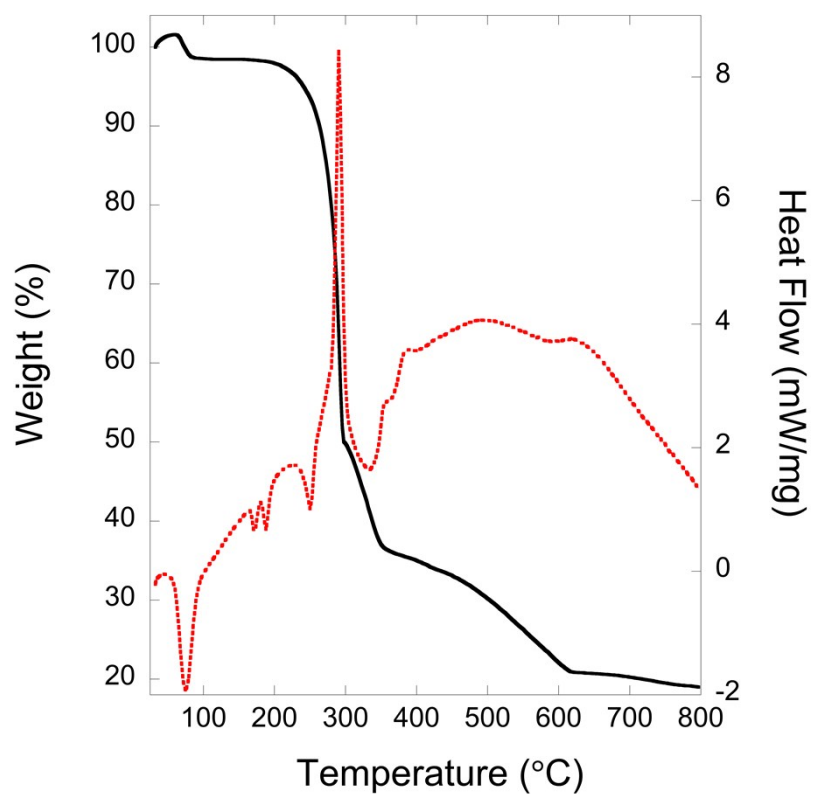


Fig. S18: Thermogravimetric (continuous black line) and differential thermal (dotted red line) analysis obtained from $\text{Hyd}_{10}\text{Mn}_3\text{Cl}_{16}$ in air.

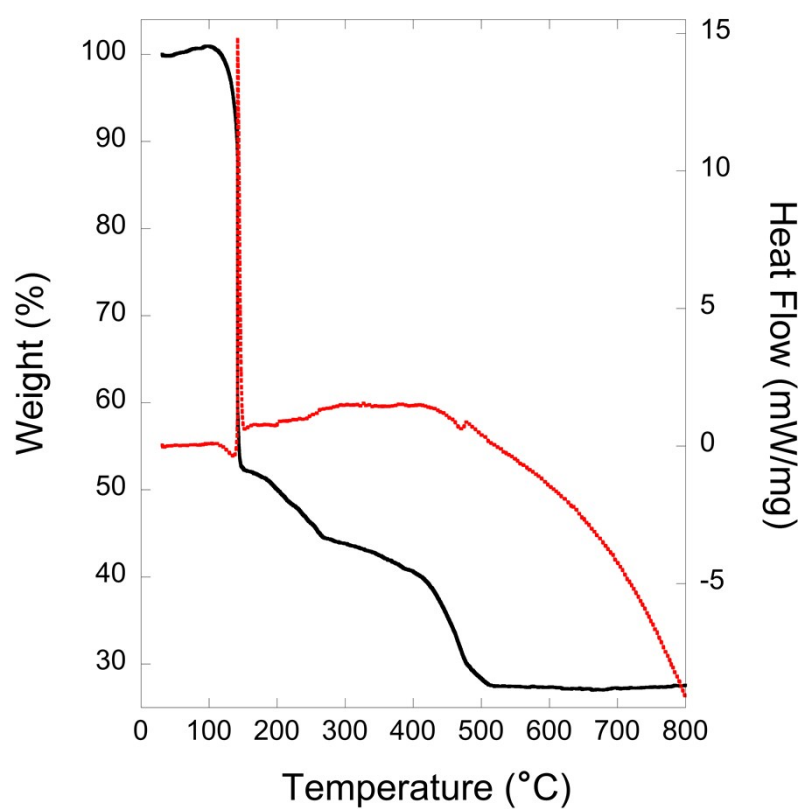


Fig. S19: Thermogravimetric (continuous black line) and differential thermal (dotted red line) analysis obtained from $\text{MHA}_2\text{CuCl}_2$ in air.

Magnetic Property Measurements

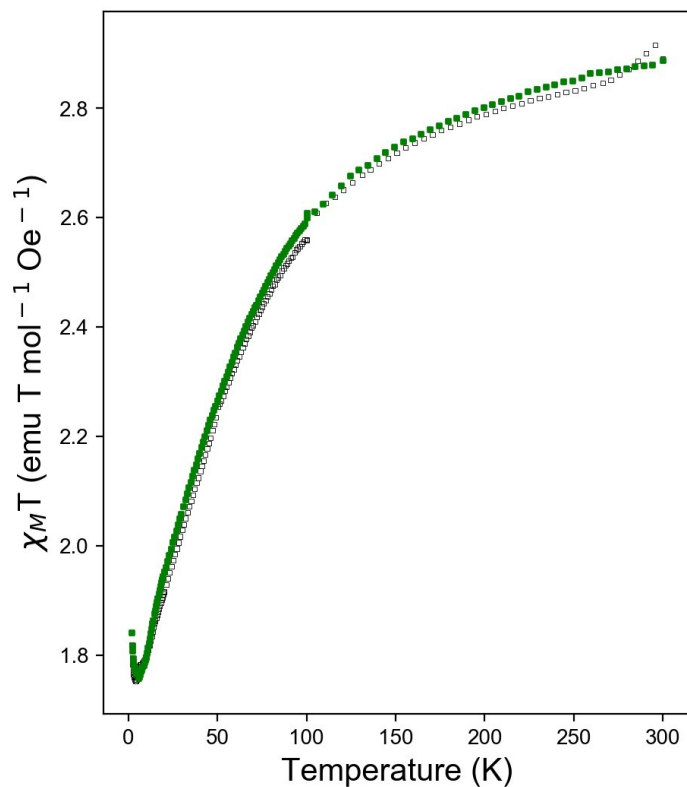


Fig. S20: Change of χT with temperature from 1000 Oe ZFC (hollow black symbols) and FC (filled green symbols) for $\text{Hyd}_2\text{CoCl}_4$.

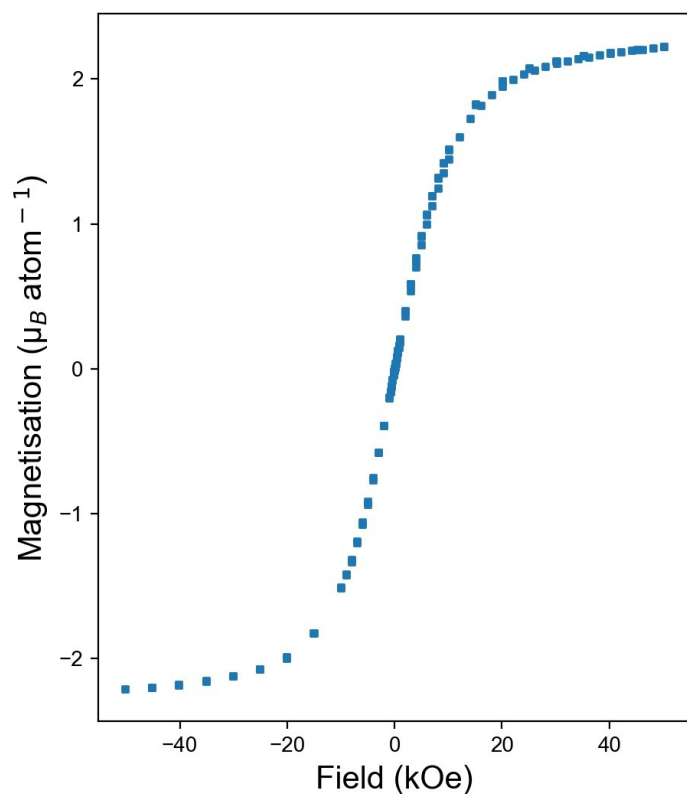


Fig. S21: Isothermal magnetisation measurement of $\text{Hyd}_2\text{CoCl}_4$ at 2 K.

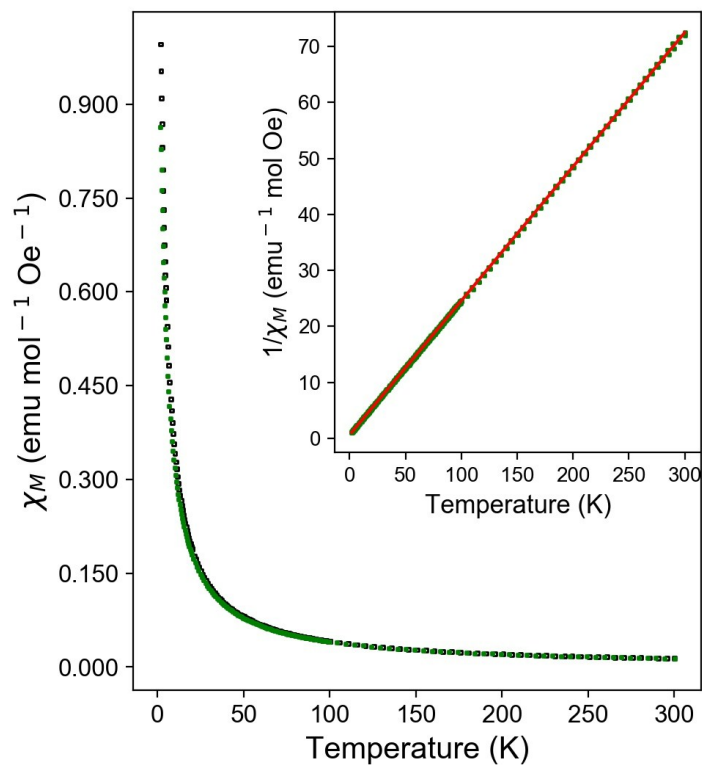


Fig. S22: Evolution of χ versus temperature for HydMnCl₃ from 1000 ZFC (hollow black symbols) and FC (filled green symbols). The insert shows inverse χ versus temperature with the red line showing a Curie-Weiss fit.

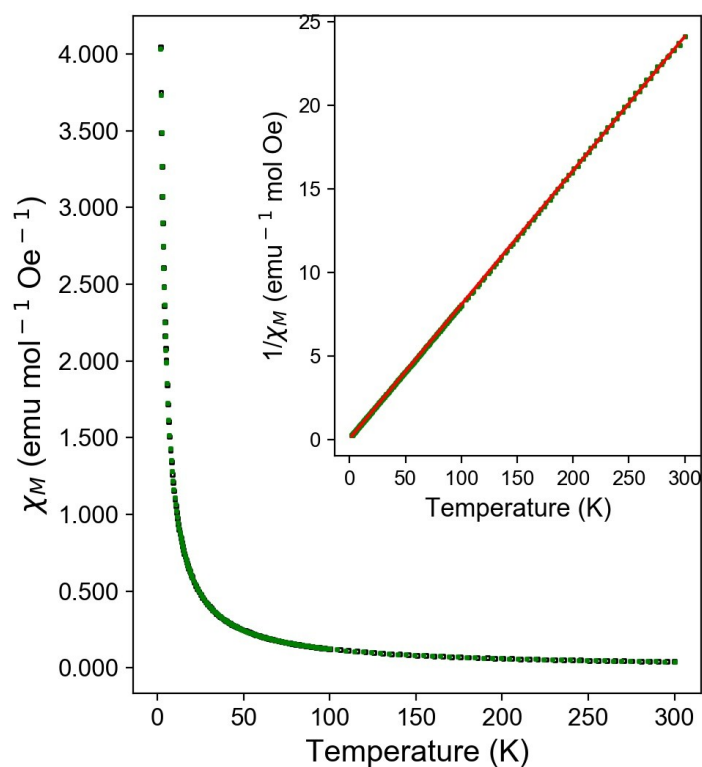


Fig. S23: Evolution of χ versus temperature from 1000 Oe ZFC (hollow black symbol) and FC (filled green symbol) for Hyd₁₀Mn₃Cl₁₆. The insert shows inverse χ versus temperature with the red line showing a Curie-Weiss fit.

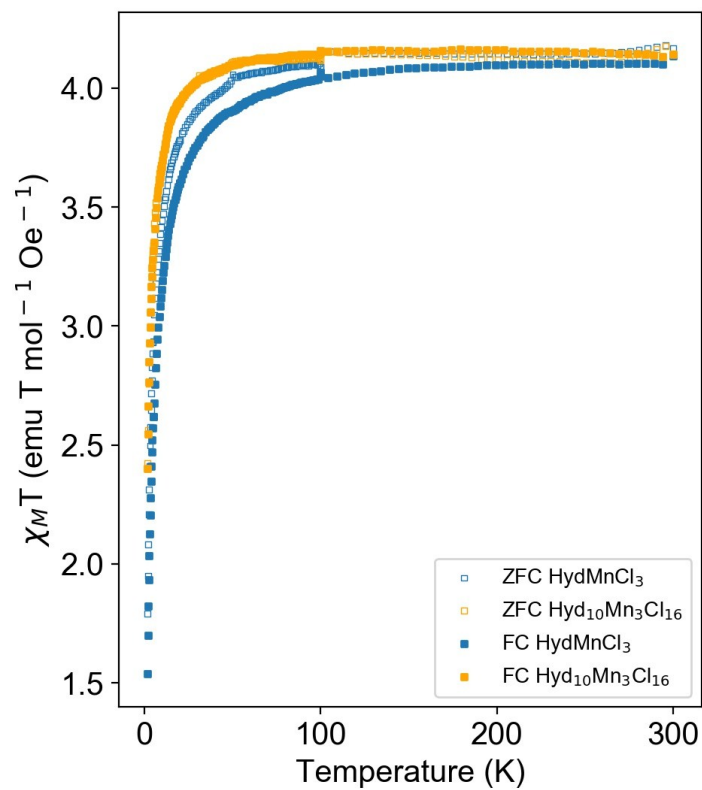


Fig. S24: Change of χT with temperature for HydMnCl_3 (blue) and $\text{Hyd}_{10}\text{Mn}_3\text{Cl}_{16}$ (orange) for 1000 Oe ZFC (hollow symbols) and FC (filled symbols) between 1.8 and 300 K.

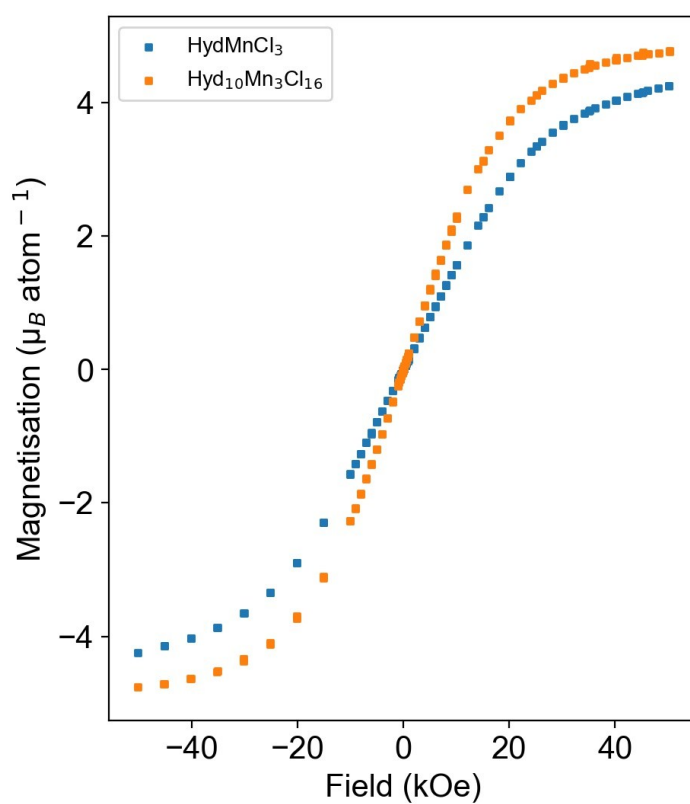


Fig. S25: Isothermal magnetisations for HydMnCl_3 (blue) and $\text{Hyd}_{10}\text{Mn}_3\text{Cl}_{16}$ (orange) at 2 K.

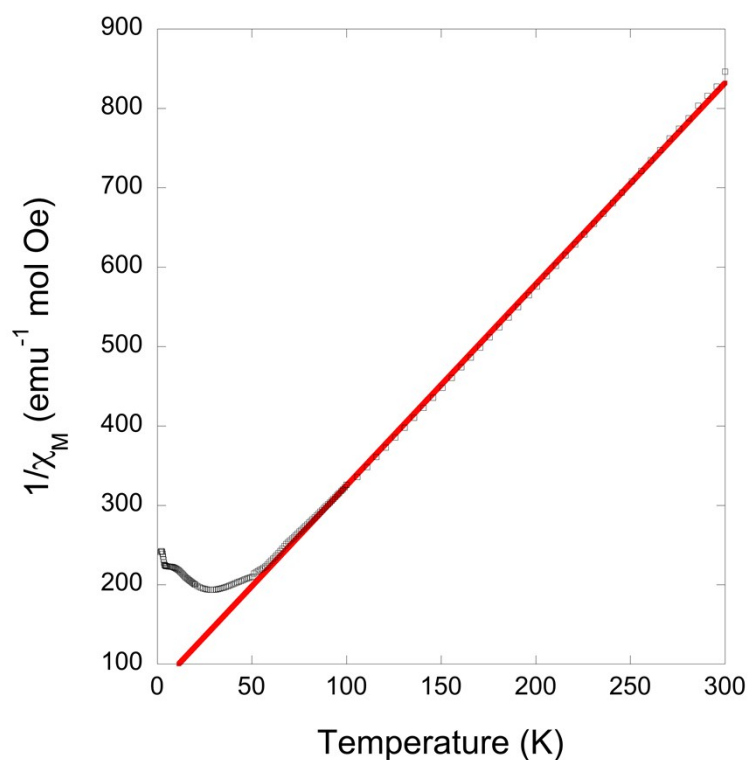


Fig. S26: Inverse χ versus temperature for $\text{MHA}_2\text{CuCl}_2$ with the red line showing a Curie-Weiss fit.

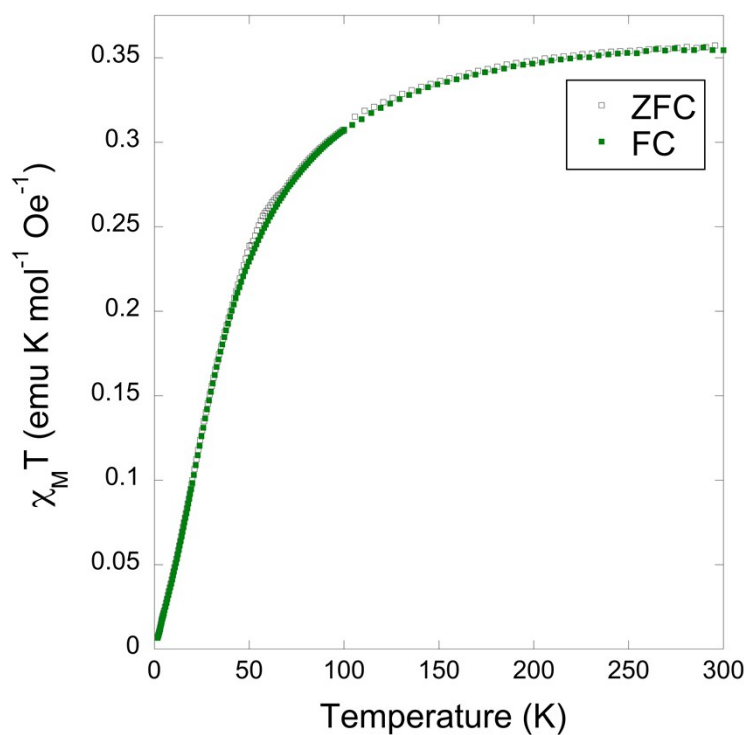


Fig. S27: Change of χT with temperature from 1000 Oe ZFC (hollow black symbols) and FC (filled green symbols) for $\text{MHA}_2\text{CuCl}_2$.

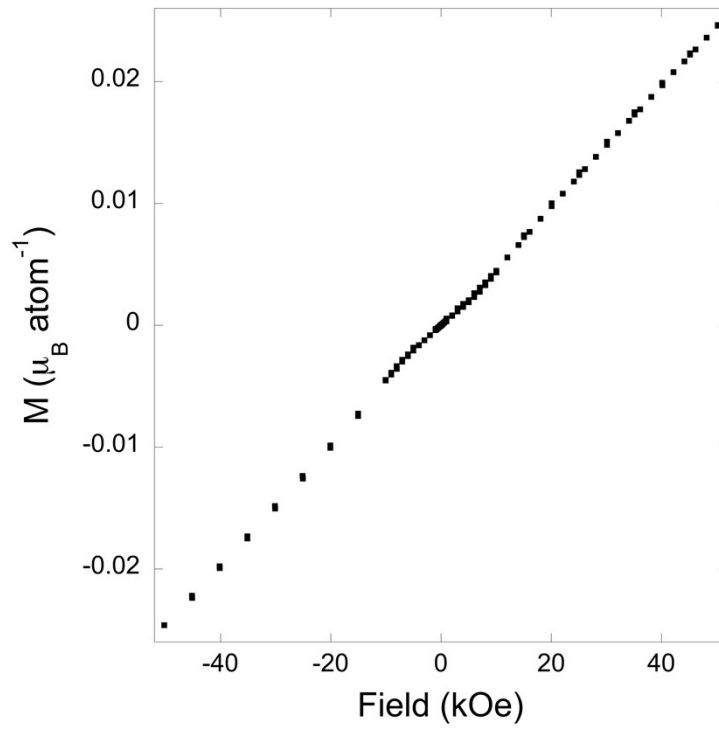


Fig. S28: Isothermal magnetisation measurement of $\text{MHA}_2\text{CuCl}_2$ at 1.8 K.